DOI: 10.1002/chem.200600392

Novel Properties from Experimental Charge Densities: An Application to the Zwitterionic Neurotransmitter Taurine

M. P. Waller,[a] S. T. Howard,*[b] J. A. Platts,[c] R. O. Piltz,[d] D. J. Willock,[c] and D. E. Hibbs*[a]

Abstract: The charge distribution of taurine (2-aminoethane-sulfonic acid) is revisited by using an orbital-based method that describes the density in a fixed molecular orbital basis with variable orbital occupation numbers. A new neutron data set is also employed to explore whether this improves the deconvolution of thermal motion and charge density. A range of molecular properties that are novel for experimentally determined charge densities are computed, including Weinhold population analysis, Mayer bond orders, and local kinetic energy densities, in addition to charge topological analysis and quantum theory of atoms-in-molecules (QTAIM) integrated properties. The ease with which a distributed multipole analysis can be performed on the fitted density matrix makes it straightforward to compute molecular moments, the lattice energy, and the electrostatic interaction energies of molecules removed from the crystal. Results are compared with high-level (QCISD) gas-phase calculations and band structure calculations employing density functional theory. Finally, the avenues available for extending the range of molecular properties that can be calculated from experimental charge densities still further using this approach are discussed.

Keywords: atoms in molecules (AIM) theory · charge density · quantum crystallography · taurine

Introduction

The advent of constrained orbital-based models being applied to experimental charge density analysis has opened up a new range of possibilities for molecular property determination from low-temperature, high-resolution elastic X-ray scattering. For example, total energies can be calculated if an idempotency constraint is applied.[1–3] Recently Whitten, Spackman, and Jayatilaka have demonstrated how selected response properties such as the dipole polarizability can be obtained.[4]

We recently reported one such alternative to the usual atom-centered multipole model for analysis experimental charge densities[5] (hereafter Paper I) which we termed MOON refinement (molecular orbital occupation number refinement). We argued that this method has the potential to describe the electron density in a molecular crystal as accurately as the multipole method[6] but in a way that has more in-built quantum-mechanical constraints than multipole refinement (e.g. the density is constrained to be positive everywhere). It offers the possibility of interpreting the experimental in-crystal density using familiar chemical concepts, for example, relating the changes in population of bonding or nonbonding molecular orbitals (MOs) to bond strengths and/or the effects of intermolecular interactions. More importantly, the orbital product-based nature of the fitted wavefunction also allows computation of properties not easily accessible from multipole-fitted densities. The use of fixed MO basis also acts as a "chemical constraint", in much the same way as use of local symmetry impacts on multipole refinement. This should be a significant advantage for treating certain non-centrosymmetric space groups that are known to be problematic for multipole studies.[7]

[a] M. P. Waller, Dr. D. E. Hibbs
Faculty of Pharmacy, University of Sydney, NSW 2006 (Australia)
Fax: (+61) 02-9351-4391
E-mail: davidh@pharm.usyd.edu.au

[b] Dr. S. T. Howard
Sansom Institute, School of Pharmacy and Medical Sciences
University of South Australia, Adelaide 5001 (Australia)
Fax: (+61) 08-8302-2389
E-mail: sian.howard@unisa.edu.au

[c] Dr. J. A. Platts, Dr. D. J. Willock
School of Chemistry, Cardiff University
Park Place, Cardiff CF10 3 AT (UK)

[d] Dr. R. O. Piltz
Bragg Institute, Australian Nuclear Science and Technology Organization, PMB 1, Menai, NSW 2234 (Australia)

Supporting information for this article is available on the WWW under http://www.chemeurj.org/ or from the author.

The study of (*Z*)-*N*-methyl-*C*-phenylnitrone reported in Paper I had some limitations: a double-ζ basis set was used throughout; the effect of anomalous scattering was corrected for in a crude way that depended on phases from the multipole model; the results were only compared with gas-phase calculations; only a limited study of the model dependence of the results was reported; and no Fourier properties were available. In fact the MOON method has the potential to be very flexible, so one goal of this study is explore the effects of different constrained models on the obtained density. Moreover in this study more flexible basis sets (e.g. including polarization functions) and basis sets that have been optimized for core densities have been utilized; anomalous scattering is corrected for in a more rigorous fashion; a DFT band structure calculation is used to provide a benchmark density; and some Fourier properties have been obtained. The effects of some different fixed MO basis models are explored, for example using different MO bases for spin-up and spin-down electrons.

A major advantage of the MOON approach over multipole models is the fact that it returns an LCAO density matrix in a basis of Gaussian orbitals. This permits access to a number of additional one-electron properties using quantum-mechanical programs such as Gaussian 03,[8] providing that the wavefunction and basis set can be interfaced appropriately. This paper illustrates how these properties may be obtained, and includes the calculation of Mayer bond orders,[9] distributed multipole analyses (DMAs)[10] and properties derivable from the DMA such as lattice energies[11] and intermolecular interaction energies,[12] along with the more familiar molecular moments, electrostatic potential and topological properties which are readily available from popular multipole refinement packages such as XD,[13] VALRAY,[14a] or JANA2000.[14b] Applying the quantum theory of atoms-in-molecules (QTAIM) methodology[15,16] to the orbitals with their adjusted occupation numbers, it is also possible to calculate QTAIM integrated properties.

The computing time required to calculate the scattering integrals needed for two-centre orbital product models makes simultaneous refinement of atomic coordinates and/or temperature factors unwieldy (they must be recalculated each time the structure is perturbed) except for the smallest of molecules. The use of neutron diffraction data is therefore an attractive option as hydrogen atoms can be located and anisotropic temperature factors for hydrogen are also determined. In this paper we report new low-temperature neutron diffraction data for taurine and utilise this in a set of MOON refinements.

Taurine (**1**) was selected for a number of reasons. A high quality X-ray diffraction dataset is available (see structure in Figure 1), and the previous multipole study[17] provides a good benchmark for some of the properties computed from the MOON refinement models. The presence of at least one second-row atom (sulfur) and substantial crystal field effects, see Figure 2, help to provide a stringent test of the MOON models. Lastly, the pharmacological significance of this neurotransmitter molecule[18–20] make it an attractive target for the computation of new properties hitherto unreported in the previously published study.

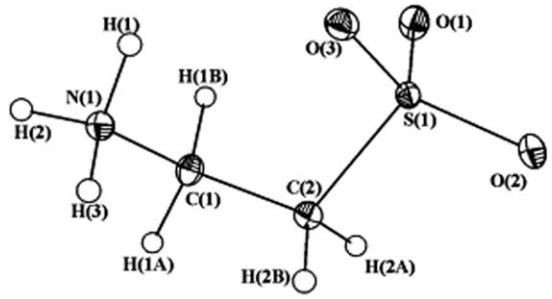

1

Figure 1. Structure of **1** (ORTEP drawing showing 50% probability ellipsoids).

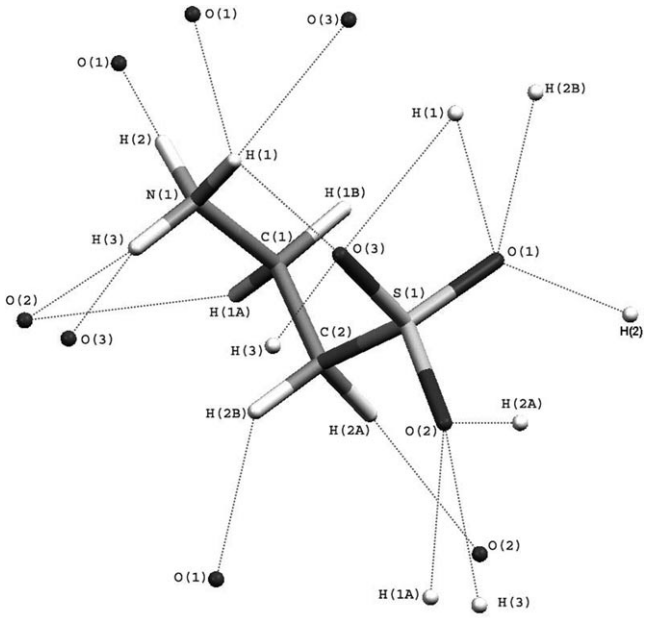

Figure 2. The intermolecular and intramolecular interactions of **1** in the solid state.

Experimental Section

X-ray data and multipole refinement: Since the X-ray data, crystal structure determination, and multipole study here have already been reported,[17] we just summarize the key details here. Multipole refinement on F with the 6108 reflections with $|F_o| > 4\sigma(|F_o|)$ gave a final agreement factor $R = \Sigma(|F_o| - k|F_c|)/\Sigma|F_o| = 0.018$ with a goodness-of-fit $S = [\Sigma w(|F_o| - k|F_c|)^2/(\text{M-N})]^{1/2} = 1.65$. The charge density was described by a total of 132 charge density parameters (multipole coefficients and kappa expansion-contraction parameters) plus 70 coordinate and temperature factor parameters.

Neutron diffraction: The single-crystal neutron diffraction data was collected at a wavelength of 1.235(1) Å using the 2TANA four-circle diffractometer at the HIFAR reactor. A single colorless crystal (1×2×5 mm) was wrapped in aluminum foil, glued to an aluminum sample pin, and mounted in the 2TANA closed-cycle helium refrigerator. The crystal was

cooled to 100(2) K (the same temperature as for the X-ray data collection). The intensities were collected and processed into integrated intensities using the ANSTO in-house programs DIFF, DIFFPLOT, and PEAKPOS. No significant trend was observed in the intensity of the two standard reflections, and so no time-dependent correction was applied to the data. A total of 3307 reflections were measured over a nine-day period in three shells of increasing Bragg angle up to a maximum of 100°. An analytical absorption correction was applied to the intensities, the correction varied from 33% to 47%. Averaging equivalent and Friedel reflections gave 956 unique reflections with $R(\text{merge}) = 0.0372$. Structure refinement using no parameter constraints and with anisotropic thermal parameters for all atoms resulted in $R1 = 0.0288$, $wR2 = 0.0660$ from a total of 128 parameters. Refinement employed anisotropic temperature factors on all atoms. Scaling of the neutron temperature factors proved necessary to correct for an evident mismatch between the actual crystal temperature in the neutron and X-ray experiments. This utilized the X-ray multipole-refined temperature factors; details of the scaling procedure used are reported in the Supporting Information. The full details of this refinement appear in the accompanying CIF.

Computational Methods

All ab initio and DFT ground-state single-point calculations at the in-crystal (X-ray refined) geometry were performed with the Gaussian 03 suite of programs[8] at various levels of theory, including Hartree–Fock (HF), the gradient-corrected BLYP functional and quadratic CI calculations (QCISD-full). Periodic (band structure) calculations at the BLYP/DZ** level were also performed by using the periodic boundary condition (PBC) method implemented in Gaussian 03. Dunning's DZ basis set was mainly used with varying levels of polarization and diffuse functions. Other Gaussian basis sets employed include STO-3G and IGLO-III[21–22] which is a large basis set with an optimal description of the core density (designed for NMR calculations).

The MOON refinement model presented in Paper I can be summarized as follows. The occupation numbers $\{n_j\}$ of K molecular orbitals $\{\varphi_j(\mathbf{r})\}$ from a variational calculation (e.g. Hartree–Fock or DFT) are refined subject to the constraints $0 < n_j < n_{max}$ and $\Sigma n_j = \text{F}(000)/Z$. Hence the basic expression for the electron density is given by Equation (1)

$$\pi(\mathbf{r}) = \sum_{j=1}^{K} n_j \phi_j(\mathbf{r})^* \phi_j(\mathbf{r}) \tag{1}$$

The MOs are expanded in a basis of contracted Gaussian atomic orbital functions. The calculated structure factor associated with this model density can be written as Equation (2), where the c_{jl} values are the fixed MO expansion coefficients; $\mathbf{r}_{lm}$ is the position vector of the lm^{th} basis function product; and T_{lm} is its temperature factor: T_{lm} is estimated as the average of the temperature factors for the two atoms on which a given basis function pair are centered. The integrals $<\chi_l|e^{2\pi i\mathbf{s}\cdot\mathbf{r}}|\chi_m>$ are basis function product Fourier transforms, and in this work are computed by using the algorithm according to Barua and Weyrich[23] at fixed crystallographic coordinates and temperature factors.

$$F_c'(\mathbf{s}) = \sum_{j=1}^{K} n_j \sum_{symm} \sum_{l=1}^{K} \sum_{m=1}^{K} c_{jl} c_{jm} <\chi_l|e^{2\pi i\mathbf{s}\cdot\mathbf{r}}|\chi_m> \exp(2\pi i\mathbf{s}\cdot\mathbf{r}_{lm}) T_{lm}(\mathbf{s}) \tag{2}$$

In Paper I, the MOON refinement models utilized all the occupied and virtual orbitals from a HF or Kohn–Sham (KS) calculation. The refinement procedure then partially depopulated the orbitals that would have been doubly occupied in the HF or KS calculation and shifted this electron density into the virtual MOs (parallels can be drawn with this procedure and carrying out a full configuration interaction calculation in the basis of canonical orbitals). This same model (hereafter MOON I) has also been employed here for analyzing the taurine data. In addition, in this paper we explore two new types of model (MOON II & IIII). In the first of these, only the populations of HF or KS occupied orbitals are varied (i.e. the virtual orbitals are not utilized at all). Since this represents a reduction of flexibility, the third model (MOON III) retains the feature of varying only HF or KS occupied orbital populations but effectively doubles the size of the MO basis used by mixing the spin-up orbitals from for example, a HF calculation with the spin-down orbitals taken from another single point calculation (e.g. KS).

Two sets of coordinates and temperature factors have been used in this study: 1) from the published X-ray multipole study and 2) from the refinements of neutron scattering data, reported in this paper. The MO coefficients are taken from gas-phase single-point HF or Kohn-Sham (KS) DFT calculations performed with the Gaussian 03 program, using one or the other of these sets of coordinates.

Equation (2) contains no explicit contribution for anomalous dispersion, which arises principally from core orbitals. The approach that has been employed in MOON is to (optionally) include the same amplitude and phase shifts used to correct atomic scattering factors, taken from the latest *International Tables for Crystallography*.[24] So to the structure factor calculated with Equation (2) the following term is added which gives an overall model structure factor $F_c(\mathbf{s}) = F_c'(\mathbf{s}) + F_c''(\mathbf{s})$, where $F_c''(\mathbf{s})$ is given by Equation (3).

$$F_c''(\mathbf{s}) = \sum_{k=1}^{Natoms} [f_k' + f_k''] T_k(\mathbf{s}) \exp(2\pi i\mathbf{s}\cdot\mathbf{r}_k) \tag{3}$$

The refinement is based on χ^2 [Eq. (4)] utilizing a combination of steepest-decent and Monte-Carlo algorithms, and is carried out until no significant further reduction in χ^2 could be achieved. Neutrality of the unit cell (and for each individual molecule) is restored at the end of each perturbation of occupation numbers by randomly choosing an orbital and adjusting its occupation number appropriately.

$$\chi^2 = \frac{1}{N} \sum_s w_s (|F_o(\mathbf{s})| - k|F_c(\mathbf{s})|)^2 \tag{4}$$

The occupation numbers obtained in this way are used to compute a density matrix according to Equation (5), where the index k runs over all the orbitals whose occupation numbers have been refined.

$$P_{ij} = \sum_k n_k c_{ik} c_{jk} \tag{5}$$

This is used to generate a Gaussian 03 formatted checkpoint file, which enables the results of the charge density analysis to be analyzed with the Gaussian 03 program and/or with any program that can read this file. Mayer bond orders were computed with BORDER.[25] Topological analysis of computed electron densities (ρ) was performed using AIM2000.[26] Gaussian 03 was used to compute the molecular moments in the Cartesian frame generated from the metric matrix and unit cell. Distributed Multipoles up to rank 4 (hexadecupole) were obtained by using the utility program GDMA.[27] The lattice energy (i.e. interaction energy per molecule with the infinite crystal) was computed by using a modified version of DMAREL,[11] which employs the DMA for the electrostatic contribution combined with an atom–atom potential model for nonbonded interactions. The interaction potential energy surface of a water molecule (gas-phase HF/DZ** level) with a taurine molecule removed from the crystal was explored by using ORIENT.[12] Molecular electrostatic potential (MEP) isosurfaces were produced by using the CUBEGEN utility associated with Gaussian 03 and visualized with gOPENMOL.[28] Fourier maps are produced from two-dimensional grid files produced by the MOON program using the CONTORPG program.[29]

Results

Effect of AO basis set size: Here we employed the original model (MOON I) with gas-phase HF MOs orbitals. Paper I

used Dunning's double-ζ (DZ) basis without polarization functions. The addition of polarization functions (DZ**) yields a significant improvement in the refinement statistics (Table 1). This is perhaps unsurprising given that taurine contains a sulfur atom, and it is widely accepted that sulfur requires d-type polarization functions to achieve an adequate representation of the electron density—in this case the description of the dπ–pπ character of S–O bonds. While polarization functions significantly improve refinement statics, diffuse functions (DZ++**) evidently have an insignificant effect. The STO-3G results are included to show the full range of effect of basis size on refinement statistics, and would not normally be appropriate except perhaps for very large molecules.

Table 1. Refinement statistics for different basis sets, computed before refinement (i.e. from the Hartree–Fock starting guess) and after MOON I refinement.

Basis set		K	χ^2	R
STO-3G	initial	46	1.6581	0.0373
	final		0.7221	0.0273
DZ	initial	92	0.7461	0.0250
	final		0.4784	0.0214
DZ**	initial	155	0.6111	0.0230
	final		0.3812	0.0200
DZ++**	initial	190	0.6075	0.0230
	final		0.4457	0.0213
IGLO-III	initial	393	0.5801	0.0221
	final		0.3899	0.0197

It might be expected that large basis sets optimized for core density such as IGLO-III would give significantly improved refinement statistics. In fact the results showed that using the IGLO-III basis does not significantly improve on the DZ** statistics (slightly lower R value but higher χ^2) despite the fact that the basis size has more than doubled. Based on these results, the DZ** basis is an attractive choice, given the trade-off between basis size and the time required for computation of integrals.

Before leaving this section, we note that the R value is not a particularly sensitive indicator of refinement quality when using high-quality wavefunction representations of the charge density. The quality of the charge density derived from a good-quality gas-phase wavefunction is such that refinement does not produce a very substantial lowering in R value (see for example, DZ** results which change from 0.023 to 0.020 on refinement). However, the χ^2 statistic registers a much bigger change, almost halving in magnitude (i.e. compared to the initial HF or KS value).

Effect of the fixed MO basis: The influence of the fixed MO basis (e.g. HF canonical orbitals, KS orbitals or some other choice such as Boys-localized MOs) was explored in Paper I. The preliminary finding was that the KS orbital basis displayed a marked improvement over HF or localized orbitals; and as the KS orbitals already encapsulate electron correlation with integer occupation numbers, this seems reasonable. However due to the limited (DZ) basis employed in that study it seems pertinent to briefly reinvestigate this here. Statistics for refinement using different MOs with a fixed (DZ**) basis set are shown in Table 2. It should be noted that, although three KS functionals were tested (SVWN, BLYP, and B3LYP), the differences in refinements statistics were very small, so results are presented for just one of these (BLYP).

Table 2. Refinement statistics for various MOs using the DZ** basis set.

Type of fixed MO basis		χ^2	R
HF	initial	0.6111	0.0230
	refined	0.3812	0.0200
localized (Boys)	initial	0.6111	0.0230
	refined	0.3601	0.0208
BLYP	initial	0.6004	0.0223
	refined	0.4179	0.0207

There is a small difference in refinement statistics corresponding to HF and BLYP MOs: HF gives slightly lower refined χ^2 and R, although (as would be expected) BLYP gives better statistics prior to refinement. A refinement using localized orbitals (derived from the the HF density) is also reported in Table 2. These localized orbitals actually give the lowest χ^2 (but the highest R value). In general it is encouraging that the final R values with three different sets of orbitals are almost identical, which suggests that all three fixed MO bases contain enough flexibility to describe the scattering data.

Effect of different MOON models: Table 3 reports the refinement statistics with the same gas-phase HF/DZ** MOs and three different refinement models MOON I–III, as described in the Computational Methods section. MOON I model is the most flexible model, since it uses the 33 occupied MOs plus 132 virtual MOs from a DZ** gas-phase calculation, that is, a total basis size of 155 MOs for describing the density. This compares with MOON II which just varies the occupation numbers of the 33 HF-occupied MOs (basis size = 33 MOs) and MOON III which utilizes the 33 spin-up occupied MOs from a HF/DZ** single-point calculation and the corresponding 33 spin-down occupied MOs from a single-point BLYP calculation (total basis size = 66 MOs). Predictably MOON I gives the best refinement statistics of the orbital models. Model III registers a small improvement

Table 3. Model dependence of MOON refinement using HF/DZ** MOs; comparison with the published multipole study.

	K	χ^2	R
before refinement	155	0.6111	0.0230
MOON I	155	0.3812	0.0200
MOON II	33	0.4937	0.0227
MOON III	66	0.4752	0.0228
multipole[17]	202	–	0.018

in the χ^2 refinement statistic compared to Model II, due to the increased flexibility. We note that the original multipole study gives the best R value; however it uses more parameters than any of the orbital models, and the coordinates and temperature factors being used here were optimized for that multipole refinement.

The MO occupation numbers obtained for Model I are illustrated in Figure 3. One noteworthy feature is the very small changes of the core orbital occupation numbers (n_1–n_{11}) from the initial values of 2.0, except for one notable exception. This is orbital $n_8=2.61$, which is mostly a localized 2s-type AO on the sulfur atom of the -SO_3^- group. A couple of the valence HF-occupied MOs are strongly depopulated by the refinement procedure ($n_{12}=0.788$ and $n_{23}=0.811$, compared to initial values of $n=2$), and several valence MOs have increased their occupation numbers well above

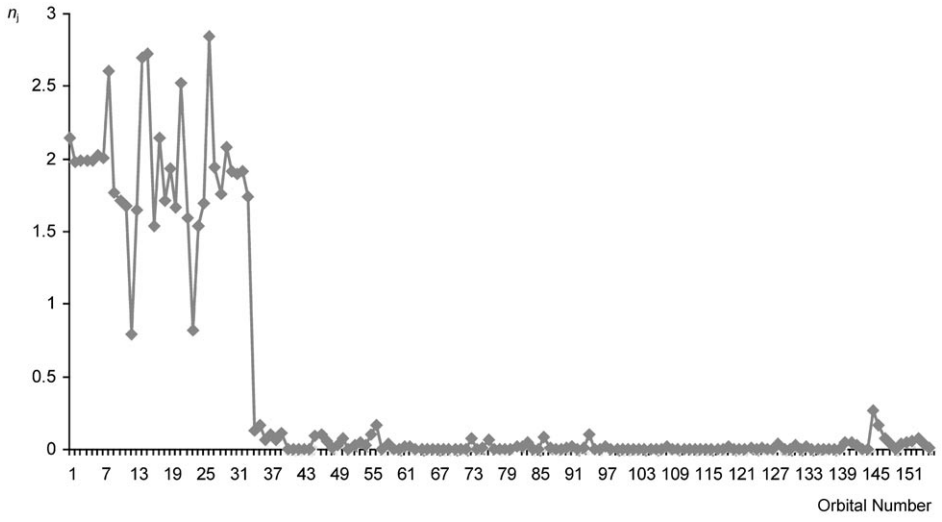

Figure 3. Orbital occupation numbers for refinement Model I (DZ** basis).

2.0 ($n_{14}=2.69$, $n_{15}=2.72$, $n_{21}=2.51$, $n_{26}=2.84$). Although many of the HF virtual orbitals have become populated their occupation numbers are mostly small (less than 0.2 electrons), the one exception being $n_{145}=0.27$.

The MO occupation numbers obtained for Model II are illustrated in Figure 4. The pattern of population/depopulation is very similar to that for MOON I for the occupied orbitals.

Figure 5 displays the refined occupation numbers for MOON III, which mixes HF/DZ** and KS/DZ** MOs. Interestingly the HF and KS show very similar trends of population/depopulation, except that the occupation numbers of the KS orbitals show greater swings in magnitude.

In principle, it might be possible to interpret the largest changes in MO occupation numbers, for example, by considering the inter/intramolecular interactions present. In practice this is difficult since changes in the occupation number of the (gas-phase) MOs are also related to the effects of electron correlation in the experimental density. Taurine has

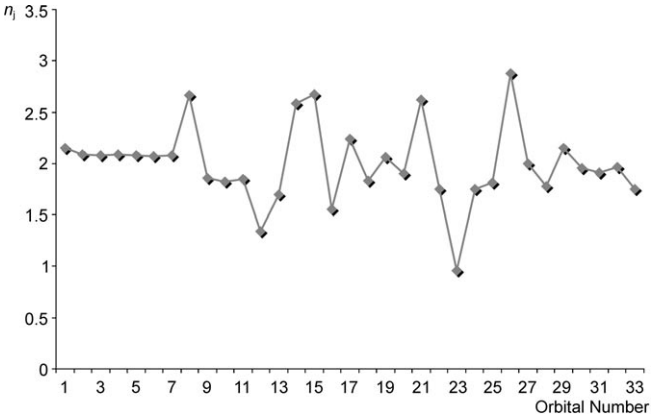

Figure 4. Orbital occupation numbers for refinement Model II (HF/DZ** basis).

a strong intramolecular N–H···O hydrogen bond, but due to the presence of two strongly polar groups also has a large number of intermolecular hydrogen bonds.

The MOs that undergo the largest population/depopulation are shown in Figure 6 in squared (probability density) form. Refinement increases the population of the sulfur 2s-type localized orbital to $n_8=2.68$, and two of the other valence orbitals localized on the -SO_3 group (14 and 15) also increase their populations substantially. The population of MO 12, which distributes density evenly over both the -NH_3 and SO_3 groups, falls to just $n_j=0.78$. The HF virtual orbital which has the highest occupation number following MOON refinement is MO 145,

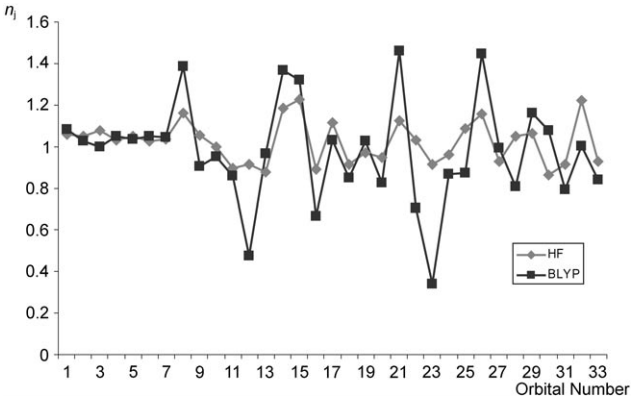

Figure 5. Orbital occupation numbers for refinement Model III (DZ** basis).

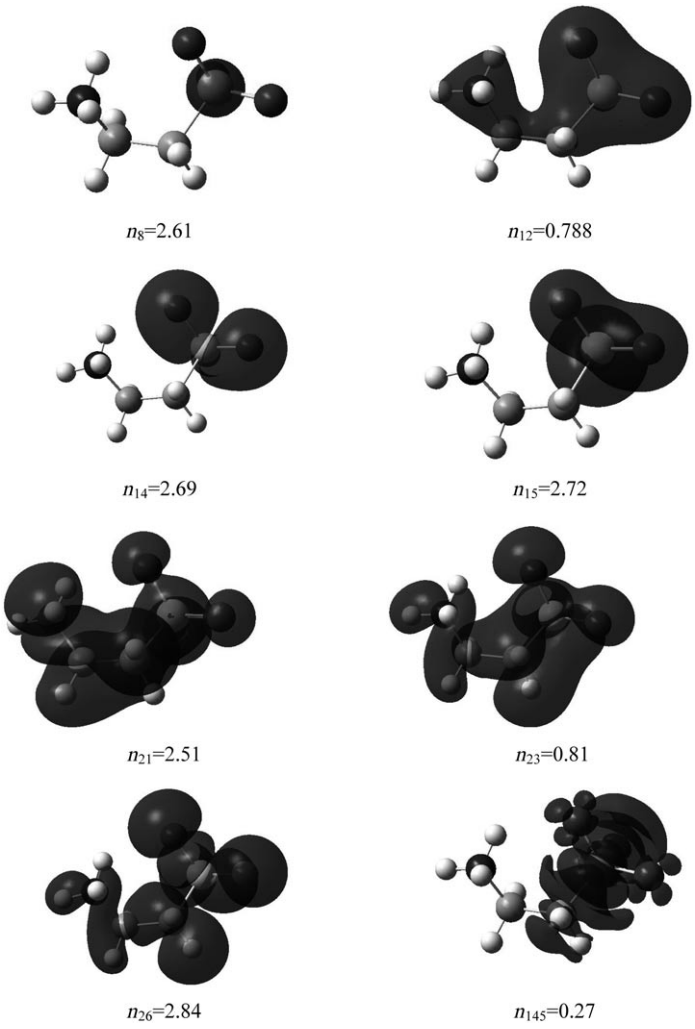

Figure 6. Probability distributions (square of the MOs) of the MOs showing the largest occupation number changes following HF/DZ** refinement (plotted at isovalue 0.02 a.u.).

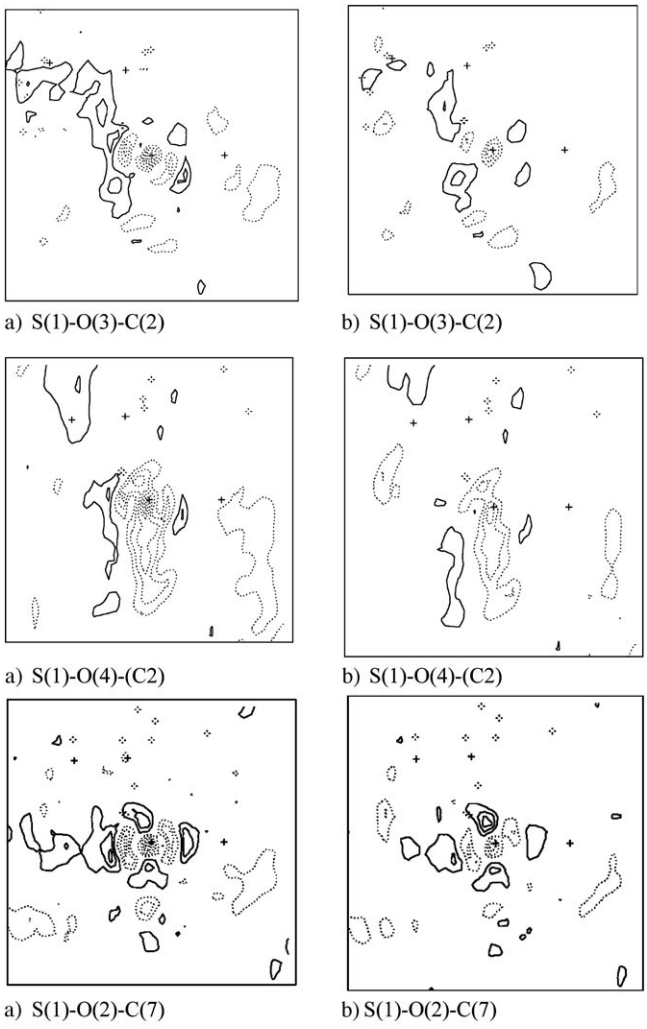

Figure 7. The 2D residual density plots (Contours at 0.1 e Å^{-3}) for the three S-O-C planes of the -SO_3 group: a) Initial HF/DZ**wavefunction; b) MOON I refinement in the HF/DZ** basis. Crosses mark the three atoms which define the plot; sulfur is at the map center in all cases.

which has a complex structure localized on the -SO_3 group (3p on sulfur in linear combination with d-type polarization functions on the oxygen atoms). Although it isn't possible to chemically interpret these various changes, this example does illustrate how the use of a fixed MO basis consisting of core, valence and virtual MOs can leads to a very detailed redistribution of electron density in much the same way as the atom-centered multipole model.

Fourier synthesis has been used to create 2-D maps of the residual electron density before and after MOON refinement. The sulfur atom is invariably associated with the largest residual density, so Figure 7 shows the residual density for three planes containing the sulfur, its attached carbon, and each of the oxygen atoms. In each case two maps are shown: a) residual based on the initial HF/DZ** density b) residual following MOON I refinement. The noteworthy point is that the residual features are generally decreased in the (b) maps corresponding to the MOON-refined density; this is particularly true in regard to the feature localized around the sulfur atom core.

Properties of zwitterionic taurine: The real advantage of using a MO-based model of the electron density is the ability to compute a wide range of properties, some of which are not attainable from multipole refinement. The following section illustrates the calculation of both these novel properties and also some more traditional properties such as the molecular dipole moment, which are readily available from most multipole charge density codes. All the properties in this section have been obtained by refinement using the fixed coordinates and temperature factors from the published multipole study. The effect of switching to neutron coordinates and temperature factors is discussed later.

Weinhold natural population analysis (NPA): Weinhold's natural population analysis[30] provides an efficient method for producing chemically intuitive partial atomic charges

that are not accessible from multipole analysis. This also makes it easy to compare atomic charges obtained from experiment and theory. Table 4 reports NPA charges for several theoretical reference densities and the three MOON-refined models discussed earlier. Relative to the gas-phase HF density, reduction in NPA charges of the atoms in the -SO_3 group is predicted by both gas-phase QCISD and PBC calculations, and supported by the refinement models (particularly the most flexible model I). We also note that O3, which is involved in the strong intramolecular H-bond, shows the biggest reduction in charge in both the periodic (PBC) calculation and the MOON I refinement.

Table 4. Weinhold natural population analysis for taurine (DZ** basis).

NPA charges	HF	QCISD	PBC	MOON I	MOON II	MOON III
S1	2.55	2.35	2.28	2.03	2.18	2.16
O1	−1.10	−1.02	−0.97	−1.06	−1.23	−0.85
O2	−1.06	−0.98	−0.92	−0.97	−1.17	-0.69
O3	−1.14	−1.07	−0.92	−1.03	−1.20	-0.81
N1	−0.77	−0.71	−0.85	−0.59	−0.64	-0.48
C1	−0.14	−0.16	−0.20	−0.08	−0.01	-0.34
C2	−0.63	−0.65	−0.67	−0.40	−0.39	−0.53
H1	0.49	0.47	0.47	0.43	0.51	0.29
H2	0.44	0.43	0.49	0.40	0.49	0.23
H3	0.45	0.44	0.48	0.39	0.48	0.23
H4	0.24	0.24	0.24	0.18	0.23	0.13
H5	0.20	0.21	0.25	0.22	0.24	0.20
H6	0.25	0.25	0.27	0.33	0.33	0.30
H7	0.21	0.21	0.27	0.15	0.17	0.15

Turning attention to the -NH_3^+ group, theory (including PBC theory) is predicting little change here compared to the HF gas-phase wavefunction. The three MOON models show significant differences here; but again the closest to the theoretical predictions is model I (consider for example, the -NH_3 group charge: +0.61, HF gas-phase; +0.59, PBC; +0.63, MOON I).

In all the calculated and MOON-refined densities the NPA charge of H1 (involved in the intramolecular H-bond) is largest.

Mayer bond orders: Calculation of Mayer bond orders (Table 5) requires just the fitted density matrix and the AO overlap matrix. In the closed-shell case the bond order between atoms A and B is given by Equation (6)[17], where the two summations are over AO basis functions centered on A and on B, respectively.

$$n_{AB} = \sum_{i \in A} \sum_{j \in B} (PS)_{ij}(PS)_{ji} \qquad (6)$$

In this case, our two "reference" electron densities behave differently. Electron correlation at the QCISD level gives rise to a very small reduction in most bond orders (i.e. compared to the HF level) while electron correlation plus the effects of the crystalline environment at the B-LYP level have a mixed effect. For example, the bond order increases in the bond S1−O3 (which is involved in the strong intramolecular H-bond) but reduces in the other two S−O bonds. The MOON I refinement mostly results in small reductions of bond order compared to the HF initial density, in line with the QCISD results. MOON I refinement also introduces some significant differences in the bond orders of pairs of bonds which are virtually identical in all reference densities, for example, C2−H6 and C2−H7. In fact this would appear to be an aphysical effect given that these are C−H bonds which only interact very weakly with the environment. More likely it is due to deficiencies in the (isotropic) thermal motion model used in the X-ray multipole study. The other two refinement models II and III predict rather larger increases in the bond orders of all the S−O bonds.

Table 5. Mayer bond orders for various model and refined densities.

	HF	QCISD	PBC	MOON I	MOON II	MOON III
S1−O1	1.53	1.50	1.44	1.53	1.66	1.69
S1−O2	1.62	1.59	1.59	1.60	1.74	1.76
S1−O3	1.44	1.40	1.47	1.38	1.54	1.56
N1−C1	0.8	0.78	0.94	0.75	0.88	0.89
S1−C2	0.9	0.82	0.87	0.72	0.84	0.78
C1−C2	0.92	0.88	0.96	0.64	0.78	0.78
N1−H1	0.81	0.78	0.82	0.61	0.77	0.75
N1−H2	0.88	0.84	0.81	0.59	0.77	0.75
N1−H3	0.87	0.84	0.82	0.63	0.79	0.78
C1−H4	0.95	0.89	0.91	0.79	0.93	0.92
C1−H5	0.97	0.91	0.92	0.71	0.87	0.84
C2−H6	0.95	0.90	0.89	0.66	0.73	0.76
C2−H7	0.95	0.89	0.90	0.84	0.98	0.97

The 'in-crystal' molecular dipole moment: A taurine zwitterion "extracted" to the gas phase naturally has a large dipole moment of ≈15 Debye (see the HF and QCISD results in Table 6). This was reproduced well by the previous multipole study,[17] which indicated a slight "enhancement" in the crystal, to around 17.5 Debye. (To calculate this in-crystal dipole moment, the authors of reference [26] used the approximation commonly employed in multipole studies which is to calculate the dipole moment arising from just those monopoles and dipoles for atoms belonging to one molecule in the unit cell). Here for the first time we have a PBC calculation which should help to confirm whether there is indeed any in-crystal enhancement in the dipole moment of zwitterionic taurine. However, to extract a dipole moment from the PBC calculation, it is also necessary to use some kind of partitioning scheme, for example the Hirshfeld parti-

Table 6. Molecular dipole moments (Debye).

	μ_x	μ_y	μ_z	μ_{Total}
HF	3.4	−14.8	−4.1	15.7
QCISD	3.2	−14.2	−3.6	15.0
PBC	5.1	−17.1	−3.6	18.2
MOON I	4.7	−16.1	−6.2	17.9
MOON II	5.3	−22.3	−7.7	24.2
MOON III	5.6	−22.3	−7.7	24.2

tioning scheme utilized by Whitten.[4] We found it most convenient to use an alternative approach, which is to compute a distributed multipole analysis of the wavefunction from the PBC calculation (entire contents of the unit cell, that is, four molecules) and then utilise the distributed monopoles and dipoles from just one molecule to calculate a dipole moment. This dipole moment also appears in Table 6. It is in excellent agreement with that determined in a previous multipole study, which predicted a slight (17%) dipole moment magnitude enhancement relative to gas-phase calculations.

Molecular dipole moments are easily calculated for MOON-refined densities using its interface to the Gaussian03 code. MOON I predicts a dipole moment which is in excellent agreement with the previous multipole result and with the PBC calculation.

The other two (less flexible) MOON models are out of line with all other results, predicting much larger enhancement of the dipole moment.

The lattice energy: The lattice energy is easily calculated as the total stabilization energy per molecule in the unit cell of the PBC (B-LYP/DZ**) calculation. This yields $-248\,kJ\,mol^{-1}$ using the (multipole) X-ray refined coordinates. (This is the dominant electronic contribution to the lattice energy, ignoring thermal contributions). Lattice energies may be estimated from the results of multipole refinement, using the multipoles to calculate the electrostatic part of the interaction energy in combination with an appropriate model of the nonbonded interaction energy. Indeed the computer program XDINTER, which interfaces to the XD multipole code, does exactly this.[31] It was applied to taurine in the published multipole study,[17] in which a lattice energy of $-207\,kJ\,mol^{-1}$ was reported. Here we have devised an alternative approach which is to carry out a static calculation of the lattice energy using the DMAREL code of Price and Willock,[11] replacing a gas-phase DMA for the taurine molecule with our MOON-refined DMA. (The DMAREL code was designed to predict molecular crystal structures; but it also predicts reliable lattice energies from known coordinates).

The lattice energy analysis for a DMA derived from the MOON I refinement is given in Table 7. For comparison, the results of a DMA derived from a HF/DZ** gas-phase wavefunction using the same coordinates are also listed. The increase in predicted lattice energy compared to the gas-phase wavefunction is an expected result of the slightly larger dipole moment. There is excellent agreement between the MOON I total lattice energy and the PBC calculation, which is very encouraging, given the completely different manners in which these two quantities have been derived. The discrepancy with the published multipole-derived lattice energy is surprising, and clearly doesn't arise from differences in dipole moment. It must therefore have its origin in the different atom-atom potentials used in DMAREL and XDINTER.

Table 7. Contributions to the total lattice energy [$kJ\,mol^{-1}$] from the DMAREL code, using the DMA from the HF/DZ** gas-phase wavefunction and the MOON I-refined wavefunction.

	HF/DZ**	MOON I
Ewald-summed charge–charge energy	−4778.0	−3103.0
intramolecular charge–charge energy	−4501.1	−2793.9
intermolecular charge–charge energy	−276.9	−309.2
total charge–dipole + dipole–dipole energy	62.8	63.2
higher multipole interaction energy	4.3	−11.8
total short range energy	−2.4	3.8
total lattice energy	−212.3	−254.0

Topological analysis including local kinetic energy densities: Application of AIM theory enables a detailed description of the electron density. Although a topological analysis based on a multipole-refined density has already been reported,[17] this was necessarily limited to properties derived from the density such as ρ_c and $\nabla^2\rho_c$ (we note that Abramov and coworkers[32] developed an *approximate* expression for critical point kinetic energy density H_c). The orbital model used in MOON refinements permits use of the *exact* orbital expression for the local kinetic energy density $H(\mathbf{r}_c)$ at critical points. This in turn extends the range of useful chemical properties which (in principle) are accessible from charge density studies, such as bond energies (using for example the parameterization scheme developed by Grimme,[33] or bond orders using the approach reported by Howard and Lamarche[34]).

Topological analysis was performed on the refined wavefunction file and compared to 1) the gas phase density from a QCISD/DZ** single point calculation and 2) the density from solid-state (periodic boundary calculation) calculation at the B-LYP/DZ** level.

The molecular graph depicted in Figure 8 shows that all critical points were successfully located, including the intramolecular N–H···O hydrogen bond and an associated ring critical point. Since the analyses presented in the previous section (especially the dipole moment and lattice energy analyses) suggests that MOON I is superior, we only report results for this single refinement model. Table 8 also reports topological analyses for three reference densities (HF, QCISD and PBC) all in the same HF/DZ** basis.

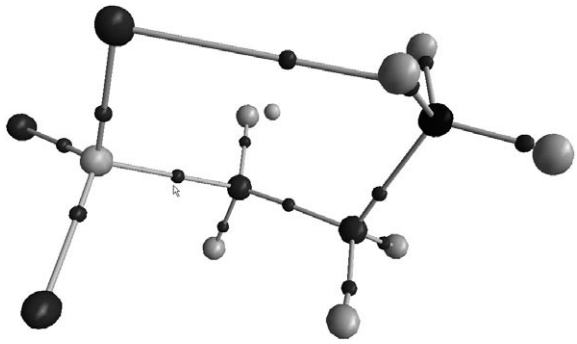

Figure 8. The molecular graph of the taurine molecule (MOON I refinement).

Table 8. Critical point topological properties (in atomic units) of taurine with various model densities compared to the MOON I refinement.

BCPs	ρ ($\mathbf{r}_c$)				$\nabla^2\rho(\mathbf{r}_c)$				$H(\mathbf{r}_c)$			
(3,−1)	HF	QCISD	PBC	MOON I	HF	QCISD	PBC	MOON I	HF	QCISD	PBC	MOON I
S1−O1	0.279	0.273	0.271	0.277	1.13	1.05	0.94	1.59	0.29	0.29	0.29	0.32
S1−O2	0.286	0.281	0.28	0.285	1.27	1.19	1.09	1.50	0.30	0.30	0.29	0.33
S1−O3	0.276	0.271	0.273	0.281	1.18	1.09	0.94	1.50	0.29	0.29	0.29	0.34
S1−C1	0.222	0.212	0.209	0.206	−0.28	−0.53	−0.46	−0.49	0.29	0.19	0.17	0.19
N1−C2	0.222	0.231	0.241	0.230	−0.64	−0.44	−0.55	−0.49	0.29	0.29	0.26	0.30
C1−C2	0.257	0.248	0.246	0.219	−0.74	−0.66	−0.62	−0.58	0.24	0.23	0.21	0.22
N1−H1	0.346	0.341	0.327	0.323	−1.94	−1.83	−1.67	−1.69	0.52	0.51	0.46	0.49
N1−H2	0.351	0.346	0.315	0.314	−1.92	−1.81	−1.59	−1.63	0.52	0.51	0.44	0.47
N1−H3	0.35	0.344	0.319	0.319	−1.92	−1.81	−1.63	−1.65	0.52	0.51	0.45	0.47
C1−H4	0.297	0.29	0.283	0.285	−1.24	−1.15	−1.06	−1.15	0.34	0.33	0.30	0.35
C1−H5	0.294	0.287	0.283	0.267	−1.18	−1.10	−1.07	−1.02	0.33	0.32	0.30	0.33
C2−H6	0.288	0.281	0.277	0.251	−1.14	−1.05	−1.01	−0.95	0.32	0.31	0.29	0.29
C2−H7	0.286	0.279	0.276	0.281	−1.10	−1.01	−1.00	−1.06	0.32	0.31	0.29	0.32
O3−H1(H-bond)	0.015	0.015	0.014	0.017	0.059	0.056	0.059	-0.057	0.00	0.00	0.00	0.00
(3,+1)												
O3-C2-H1	0.01	0.01	0.01	0.013	0.056	0.055	0.054	0.052	−0.003	−0.003	−0.003	−0.001

The QCISD (gas-phase) and PBC results suggest that the CP densities are overestimated at the HF level; hence the MOON refinement, which begins with a HF/DZ** density, should tend to decrease CP densities. Indeed the refinement process ought to decrease in all bonds except N−C; the MOON I refined density does indeed show this trend, that is, refined CP densities are moving in the direction of the two electron-correlated densities, one of which includes the effects of crystal periodicity.

A comparison of the theoretical $\nabla^2\rho$?values in Table 4, which characterize ionicity/covalency, shows that the QCISD and PBC densities tend to reduce the ionic character of many bonds ($\nabla^2\rho$ becomes less positive) compared to the initial HF density—this could be rationalized by the fact that HF wavefunctions have an overestimated ionicity. In fact the refined values display the opposite trend, with the positive $\nabla^2\rho$ values for bonds in the HF initial density becoming more positive in the refined density. While this is disappointing it does correspond with similar observations from many multipole charge density studies. It had been concluded that this effect probably has its origin in the current multipole parameterizations used, which tend to shift the positions of CPs relative to theoretical reference densities. The fact that a similar effect is seen here seems to reopen this debate, since we are using a quite different, fixed MO basis parameterization of the charge density.

With regard to the CP kinetic energy densities (H_c) there are two noteworthy differences between the HF gas-phase density and the PBC density. First, the energy density in the S−C bond drops dramatically in the latter. Second, the energy density in the N−H bonds is also significantly lower in the latter. Both of these features are closely reproduced by the MOON refinement.

QTAIM charges: The partitioning scheme results in open systems (atomic basins, Ω) separated by interatomic surfaces characterized by their normal vectors $\mathbf{n}(\mathbf{r})$, where $\nabla\rho(\mathbf{r}) \cdot \mathbf{n}(\mathbf{r}) = 0$. Integration of the appropriate property density over such basins gives rise to an AIM expectation value of the property concerned: Atomic charges and higher multipoles within the framework of QTAIM can readily be calculated using the wavefunction file produced by the MOON refinement procedure, using its Gaussian03 interface. These charges are reported in Table 9. In this case it was not possible to obtain PBC values for the QTAIM charges because of difficulties in characterizing the necessary interatomic surfaces.

Table 9. QTAIM charges (a.u.).

Q(Ω)	HF	QCISD	MOON (I)
S1	3.89	3.635	3.742
O1	−1.551	−1.459	−1.687
O2	−1.54	−1.446	−1.598
O3	−1.573	−1.487	−1.650
N1	−1.262	−1.097	−0.922
C1	0.410	0.339	0.443
C2	−0.057	−0.089	0.254
H1	0.578	0.536	0.469
H2	0.491	0.457	0.407
H3	0.506	0.472	0.409
H4	0.079	0.079	0.029
H5	0.002	0.017	0.030
H6	0.037	0.043	0.124

It is immediately evident that QTAIM and NPA charges (Table 4) display some opposite trends, for example, oxygen QTAIM refined charges are markedly more negative than their QTAIM HF gas-phase counterparts, while NPA refined charges of oxygen atoms are less negative than the HF gas-phase counterparts. However group charges show a more consistent picture. The MOON-refined NPA and QTAIM group charges for -SO_3 are −1.03 and −1.20, respectively. Similarly, the MOON-refined NPA and QTAIM group charges for -NH_3 are +0.63 and +0.37, respectively. The latter are also consistent with the ammonium group charge of +0.42 for L-alanine reported by Destro et al.[35] and +0.43 the same group in L-alanine (Howard et al.[36]). As with the NPA charges, the QTAIM charges also reveal

that the O3 and H1 atoms involved in the strong intramolecular H-bond have the highest charges (e.g. compared to the other oxygen or hydrogen atoms in the same group).

Molecular electrostatic potentials (MEPs): The MEP is frequently used in charge density studies as a tool for visualizing regions of electrophilic/nucleophilic attack[37] or likely hydrogen bond formation.[38] The extrema of electrostatic potential on the 0.001 a.u. isodensity surface is commonly plotted as a means of comparing experimentally and theoretically derived MEPs. Here the MEP has been generated for one taurine molecular removed from the crystal. The increased intensity and spatial extent of the red and blue polar groups in MOON-refined taurine is consistent with the increase in group charges (e.g. for -SO_3 the NPA charge is −0.75 for Hartree–Fock and −1.03 for MOON I) and the small increase in molecular dipole moment compared to the gas-phase. The global MEP extrema on the 0.001 a.u. isodensity surface of the MOON-refined density (Figure 9, Table 10) are also accentuated compared to the gas-phase.

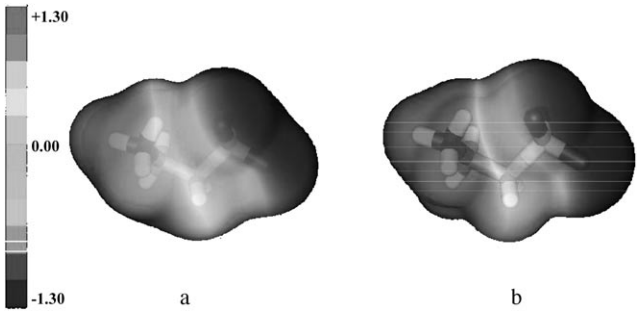

Figure 9. Molecular electrostatic potential on the 0.001 a.u. density isosurface: a) gas-phase HF/DZ**; b) MOON I/DZ**.

Table 10. MEP global extrema on the 0.001 isodensity surface.

	Gas-phase HF/DZ**	MOON I HF/DZ**
maximum in ESP (a.u.)	+0.1085	+0.1280
minimum in ESP (a.u.)	−0.0658	−0.1229

Electrostatic interaction energies for a molecule abstracted from the crystal: One of the often-stated aims of experimental charge density studies is that the results may be utilized to study intermolecular interactions: for example, by removing a molecule and its associated set of multipoles from the crystal and calculating its interaction energy with other molecules. Such an approach was pioneered by Spackman et al.[39,40] and more recently developed by Volkov et al.[32] for multipole-parameterized densities. Again, the ease with which the DMA can be generated from the results of MOON refinement makes it straightforward to carry out such studies using the ORIENT package of Stone et al. This package enables the user to search for low energy conformations on an intermolecular potential energy surface generated by DMA electrostatics combined with some model of nonbonded interactions (in this case we use the Buckingham potentials reported by Mirsky[41]). As an example of this we compute the interaction energy of a taurine zwitterion abstracted from the crystal with a "probe" water molecule (the latter represented by a HF/DZ** level DMA). For comparison we report the same analysis using DMAs derived from gas-phase wavefunctions for both species.

Minimization of the interaction energy for the MOON-refined DMA gives rise to the global minimum displayed in Figure 10. The water molecule is involved in two bridging

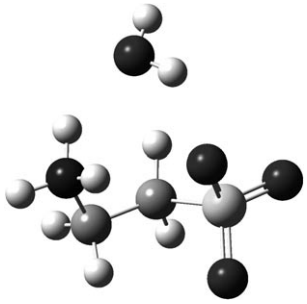

Figure 10. The global minima for the intermolecular interaction of **1** with water using the DMAs. The dashed lines represent the hydrogen-bonding interactions.

hydrogen bonding interactions with taurine, with a total stabilization energy of around −76 kJ mol^{-1}. Such interactions are presumably responsible for stabilizing the zwitterionic form in solution and in the solid state, as with amino acids.[42] In this case, using the the gas-phase DMA for taurine gives a minimum-energy structure that is almost indistinguishable from the MOON-refined case, and an interaction energy that differs by just 1 kJ mol^{-1}. There are however some more significant differences between the two models in terms of how the total Table interaction energy is broken down into electrostatic and non-bonding contributions (see Table 11).

Table 11. Intermolecular interaction energies [kJ mol^{-1}] and geometries at the global minimum calculated with ORIENT.

	HF/D95**	MOON I
electrostatic energy	−95.1	−98.7
repulsion energy	39.2	44.0
dispersion energy	−19.7	−21.6
total energy	−75.6	−76.3
H3···O1(water) distance [Å]	2.01	2.04
O3···H1(water) distance [Å]	2.03	1.98

Results based on neutron-refined coordinates and temperature factors: An entirely equivalent set of refinements (i.e. three MOON models) have been carried out using a different set of nuclear coordinates and temperature factors obtained from neutron diffraction. For the most part, this has led to very similar results to the refinements using X-ray co-

ordinates and temperature factors, so for brevity these data are reported in the Supporting Information. It was necessary to scale the neutron temperature factors for heavy atoms using the multipole-refined X-ray temperature factors as a reference; this was done using the procedure described in the Supporting Information. Here we summarize the key points arising from these refinements.

The refined orbital populations show somewhat less variation from the initial HF values of zero or two compared with the refinements based on X-ray multipole coordinates and temperature factors. Despite this, the magnitude of the molecular dipole moment obtained with neutron data was 19.0 Debye, and the lattice energy obtained was 263 kJ mol^{-1} (both very similar to the values obtained for the refinements based on x-ray coordinates and temperature factors). The ORIENT interaction energy with a test water molecule for a taurine molecule removed from the crystal was -81 kJ mol^{-1}, which again is very similar to the results obtained with X-ray coordinates and temperature factors. The difference in Mayer bond orders for bonds C2–H6 and C2–H7, which ought to be chemically equivalent, is now 0.10 compared to the 0.16 value found in the MOON refinements employing X-ray coordinates and temperature factors.

Conclusion

High-quality, low-temperature X-ray scattering charge density data have been re-analyzed for the neurotransmitter taurine, applying a new orbital-based model. The re-analysis results in a molecular dipole moment and a lattice energy that are actually more mutually consistent and also in better agreement with a periodic boundary condition calculation that was not available at the time of the original multipole analysis. For the first time, wavefunction-based measures such as Mayer bond orders and NPA charges have been used to compare an experimentally derived density with high-quality theoretical calculations (gas-phase QCISD and PBC/DFT), in addition to the usual topological analysis of the charge density. The comparison reveals that the experimental density is more similar to both of these reference densities than the Hartree–Fock density, which is used as an initial guess. A DZ(d,p) basis of molecular orbitals combined with a refinement model that varies both occupied and virtual orbital occupation numbers (but retains spin-restricted forms for the doubly occupied MOs) gives the best agreement with the theoretical densities.

Fourier residual maps in the most "troublesome" region of the molecule (i.e. the sulfur atom) verify that the refinement procedure has significantly reduced the residual compared to the same maps based on the Hartree–Fock initial density. Gross features of the charge distribution such as the dipole moment don't appear to be much affected by the choice of X-ray or neutron coordinates and temperature factors. However, the Mayer bond order analysis revealed that the charge density in bonds to hydrogen atoms may have been measurably improved (in the sense that chemically equivalent bonds give more similar bond orders) by using the neutron data.

This study has demonstrated that the MOON refinement model has at least two advantages over the well-established multipole models commonly used in charge density studies:

1) It permits calculation of properties based on orbitals and/or the density matrix which would not be accessible from multipole studies, such as Mayer bond orders, Weinhold population analyses, and local kinetic energy densities using the exact expression based on orbital gradients. These properties are readily calculated by an interface between MOON and appropriate quantum-mechanical codes (Gaussian 03 and AIM2000 have been utilized in this study).
2) The ease with which a Stone-type distributed multipole analysis (DMA) can be computed from the fitted density matrix provides a second type of interface to a range of computer codes for probing molecular interactions that utilize DMA electrostatics, such as DMAREL (for lattice energies) and ORIENT (for generalized molecular interactions).

The DMA also provides a very convenient interface for calculating molecular moments using for example, Stones's GDMA computer code.

Finally, we would like to consider whether it is possible to calculate QTAIM properties such as the atomic basin energies and (in turn) the total energy. The approach of Bader and co-workers permits not only partitioning of the equilibrium charge distribution of a molecule, but also its total energy at an atoms-in-molecules level using for example Equation (7), where the sum runs all the occupied MOs. The particular choice of partitioning delivers "atoms" (strictly the union of the nucleus and the electrons contained in the basin) which obey the virial theorem: $2G(\Omega) = -V(\Omega)$. On the face of it, it would then appear to be possible to calculate QTAIM energies with Equation (7) from MOON-refined MO occupation numbers in the fixed MO basis. This could in principle be converted to a total energy by applying the Virial theorem $E(\Omega) = -G(\Omega)$. Herein lies the first potential problem. Ab initio calculations of $E(\Omega)$ use the actual calculated Virial ratio which differs slightly from 2.0 due to the finite basis sets employed. Since we also determine the density in a finite basis the same consideration applies, but we would be unable to calculate the Virial ratio because no model of the total wavefunction is available to evaluate the total kinetic and potential energies. However if the basis is sufficiently large and flexible it might be a reasonable approximation to apply the Virial theorem "as is" and assume $2T = -V$, to obtain the total energy of the atomic basin.

$$G(\Omega) = \frac{1}{2} \sum_{k} n_k \int_{\Omega} \nabla\phi_k(\mathbf{r})^* \cdot \nabla\phi_k(\mathbf{r}) \mathrm{d}\mathbf{r} \qquad (7)$$

There is a second and more serious obstacle to doing this within the models implemented in this paper, which is the relaxation of the "Pauli constraint" (MO occupation numbers allowed to be greater than 2.0). The absence of such a constraint means that the density is no longer N-representable (i.e. in principle has some multi-determinant wavefunction associated with it). Now although this could be circumvented by applying the Pauli constraint to the occupation numbers as discussed and tested in Paper I, the same study also found that this severely restricted the flexibility of the model to describe the experimental density. Hence the utility of the MOON refinement approach for calculating more "exotic" properties such as atomic energies depends on being to develop a Pauli-constrained model which is still sufficiently flexible.

Acknowledgements

M.P.W. is grateful for the constructive suggestions regarding basis sets from Dr. T. Tuttle (Mülheim). M.P.W. would like to acknowledge the AINSE postgraduate program for financial support and the University of Sydney for generous financial support. D.E.H. and S.T.H. would like to thank the ARC for funding.

[1] S. T. Howard, J. P. Huke, C. S. Frampton, P. R. Mallinson, *Phys. Rev. B* **1994**, *49*, 7124–7136.
[2] D. Jayatilaka, *Phys. Rev. Lett.* **1998**, *80*, 798–801.
[3] J. A. Snyder, E. D. Stevens, *Chem. Phys. Lett.* **1999**, *313*, 293–298.
[4] A. E. Whitten, PhD Thesis, University of New England, **2005**.
[5] D. E. Hibbs, S. T. Howard, J. P. Huke, M. P. Waller, *Phys. Chem. Chem. Phys.* **2005**, *7*, 1772–1778.
[6] N. K. Hansen, P. Coppens, *Acta. Crystallogr. A* **1978**, *34*, 909–921.
[7] A. ElHaouzi, N. K. Hansen, C. LeHenaff, J. Protas, *Acta Crystallogr. Sect. A* **1996**, *52*, 291–301.
[8] M. J. Frisch, G. W. Trucks, H. B. Schlegel, G. E. Scuseria, M. A. Robb, J. R. Cheeseman, J. A. Montgomery, Jr., T. Vreven, K. N. Kudin, J. C. Burant, J. M. Millam, S. S. Iyengar, J. Tomasi, V. Barone, B. Mennucci, M. Cossi, G. Scalmani, N. Rega, G. A. Petersson, H. Nakatsuji, M. Hada, M. Ehara, K. Toyota, R. Fukuda, J. Hasegawa, M. Ishida, T. Nakajima, Y. Honda, O. Kitao, H. Nakai, M. Klene, X. Li, J. E. Knox, H. P. Hratchian, J. B. Cross, C. Adamo, J. Jaramillo, R. Gomperts, R. E. Stratmann, O. Yazyev, A. J. Austin, R. Cammi, C. Pomelli, J. W. Ochterski, P. Y. Ayala,K. Morokuma, G. A. Voth, P. Salvador, J. J. Dannenberg,V. G. Zakrzewski, S. Dapprich, A. D. Daniels, M. C. Strain, O. Farkas, D. K. Malick, A. D. Rabuck, K. Raghavachari, J. B. Foresman, J. V. Ortiz, Q. Cui, A. G. Baboul, S. Clifford, J. Cioslowski, B. B. Stefanov, G. Liu, A. Liashenko, P. Piskorz, I. Komaromi, R. L. Martin, D. J. Fox, T. Keith, M. A. Al-Laham, C. Y. Peng, A. Nanayakkara, M. Challacombe, P. M. W. Gill, B. Johnson, W. Chen, M. W. Wong, C. Gonzalez, J. A. Pople, Gaussian 03, Gaussian, Inc., Wallingford CT, **2004**.
[9] I. Mayer, *Chem. Phys. Lett.* **1983**, *97*, 270–274.
[10] A. J. Stone, *Chem. Phys. Lett.* **1981**, *83*, 233–239.
[11] D. J. Willock, S. L. Price, M. Leslie, C. R. Catlow, *J. Comput. Chem.* **1995**, *16*, 628–647. See http://www.ucl.ac.uk/~ucca17p/dmarelmanual/dmarel.html
[12] A. J. Stone, A. Dullweber, O. Engkvist, E. Fraschini, M. P. Hodges, A. W. Meredith, D. R. Nutt, P. L. A. Popelier,D. J. Wales, 'Orient: a program for studying interactions between molecules, version 4.5,' **2002** University of Cambridge.
[13] T. Koritsanszky, P. R. Mallinson, S. T. Howard, A. Volkov, P. Macchi, Z. Su, C. Gatti, T. Richter, L. J. Farrugia, N. K. Hansen, XD - A Computer Program Package for Multipole Refinement and Analysis of Electron Densities from Diffraction Data, **2003**, Manual Version 12.
[14] a) R. F. Stewart, M. A. Spackman, C. Flensburg, VALRAY98 Users Manual, **1998**, Carnegie-Mellon University, Pittsburgh, and the University of Copenhagen; b) V. Petříček, M. Dušek, L. Palatinus, **2000**, Jana2000, The crystallographic computing system, Institute of Physics, Praha, Czech Republic.
[15] F. W. Biegler-Koenig, R. F. W. Bader, T. H. Tang, *J. Comput. Chem.* **1982**, *3*, 317–328.
[16] R. F. W. Bader, *Atoms in Molecules: A Quantum Theory*, **1990**, Oxford University Press, Oxford.
[17] D. E. Hibbs, C. J. Austin-Woods, J. Platts, J. Overgaard, P Turner, *Chem. Eur. J.* **2003**, *9*, 1075–1084.
[18] T. C. Birdsall, *Altern. Methods Toxicol. Altern Med Rev.* **1998**, *3*, 128–136.
[19] K. Takahashi, *J. Cardiovasc. Pharmacol.* **2003**, *41*, 726–733.
[20] K. Takahashi, Y. Ohyabu, V. Solodushko, T. Takatani, T. Itoh, S. W. Schaffer, J. Azuma, *Biol. Trace Elem. Res.* **2002**, *87*, 171–182.
[21] W. Kutzelnigg, U. Fleischer, M. Schindler, *NMR Basic Principles and Progress, vol. 23*, Springer, Heidelberg, **1990**.
[22] MSL Gaussian Basis Sets from the Molecular Science Computing Facility, Environmental and Molecular Sciences Laboratory.
[23] M. Barua, W. Weyrich, *Acta Crystallogr. Sect. A* **1986**, *42*, 257–261.
[24] *International Tables for Crystallography, Vol. C*, (Ed.: E. Prince), **2005**, 255.
[25] I. Mayer, Program "BORDER", Version 1.0 (Chemical Research Center, Hungarian Academy of Sciences), Budapest, **2005**.
[26] A. J. Stone, 'GDMA: distributed multipoles from Gaussian98 wavefunctions, **1998**, Tech. rep., University of Cambridge.
[27] F. Biegler-König, *J. Comput. Chem.* **2002**, *23*, 1489–1494.
[28] See http://www.csc.fi/gopenmol/).
[29] See http://www.chemistry.mcmaster.ca/aimpac/imagemap/imagemap.htm.
[30] A. Reed, R. Weinstock, F. Weinhold, *J. Chem. Phys.* **1985**, *83*, 735–746.
[31] Y. A. Abramov, *Acta Crystallogr. Sect. A* **1997**, *A53*, 264–272.
[32] Y. A. Abramov, A. Volkov, G. Wu, P. Coppens, *J. Phys. Chem. B* **2000**, *104*, 2183–2188.
[33] S. Grimme, *J. Am. Chem. Soc.* **1996**, *118*, 1529–1534.
[34] S. T. Howard, O. J. Lamarche, *J. Phys. Org. Chem.* **2003**, *16*, 133–141.
[35] R. Destro, R. E. Marsh, R. Bianchi, *J. Phys. Chem.* **1998**, *92*, 966–973.
[36] S. T. Howard, M. B. Hursthouse, C. W. Lehmann, E. A. Poyner, *Acta Crystallogr. Sect B* **1995**, *51*, 328–337.
[37] P. Politzer, J. S. Murray, M. Concha, *Int. J. Quantum Chem.* **2002**, *88*, 19–27.
[38] A. D. Buckingham, P. W. Fowler, *Can. J. Chem.* **1985**, *63*, 2018–2025.
[39] M. A. Spackman, *J. Chem. Phys.* **1986**, *85*, 6579–6586.
[40] M. A. Spackman, H. P. Weber, B. M. Craven, *J. Am. Chem. Soc.* **1998**, *120*, 775–782.
[41] K. Mirsky, "The determination of the intermolecular interaction energy by empirical methods" in *Computing in Crystallography*, (Eds.: R. Schenk, R. Olthof-Hazenkamp, H. van Koningsveld , G. C. Bassi), **1978**, *169*, Delft University Press.
[42] S. J. Xu, M. Nilles, K. H. Bowen, *J. Chem. Phys.* **2003**, *119*, 10696–10701.

Received: March 20, 2006
Published online: July 6, 2006

